

Path-tracing Monte Carlo Libraries for 3D Radiative Transfer in Cloudy Atmospheres

Najda Villefranque^{1,2}, Fleur Couvreur¹, Richard Fournier², Stéphane Blanco²,
Céline Cornet³, Vincent Eymet⁴, Vincent Forest⁴, Jean-Marc Tregan²

¹Centre National de Recherches Météorologiques (CNRM), UMR 3589 CNRS, Météo France, Toulouse

²Laboratoire Plasma et Conversion d'Énergie (LAPLACE), UMR 5213 CNRS, Université Toulouse III

³Univ. Lille, CNRS, UMR 8518 - LOA - Laboratoire d'Optique Atmosphérique, F-59000 Lille, France

⁴Méso-Star, Toulouse, France

Key Points:

- Independent path-tracing libraries for radiative-transfer Monte Carlo codes for cloudy atmospheres
- Null-collision algorithms and computer graphics techniques to treat complex geometries and volumes
- Example of accurate three-dimensional radiation calculations to evaluate and tune parametrizations

arXiv:1902.01137v1 [physics.comp-ph] 4 Feb 2019

Corresponding author: Najda Villefranque, najda.villefranque@gmail.com

Abstract

Interactions between clouds and radiation are at the root of many difficulties in numerically predicting future weather and climate and in retrieving the state of the atmosphere from remote sensing observations. The large range of issues related to these interactions, and in particular to three-dimensional interactions, motivated the development of accurate radiative tools able to compute all types of radiative metrics, from monochromatic, local and directional observables, to integrated energetic quantities. In the continuity of this community effort, we propose here open-source radiative tools based on Monte Carlo algorithms. These tools are designed and distributed as a set of modular, independent libraries allowing the rapid design of specific codes for each new applicative requirement. Besides the implementation of state-of-the-art data access, parallelization and ray-casting acceleration techniques, we make use of integral formulations and null-collision algorithms to handle complex heterogeneous cloudy fields. Three example algorithms are described to illustrate the diversity of questions that can be addressed with these tools: rendering of synthetic images, analysis of transmission under a cloud and its sensitivity to an optical parameter, and assessment of a parametrization of 3D radiative effects of clouds. We apply them in realistic shallow cumulus fields output from Large Eddy Simulations.

1 Introduction

Radiative transfer, in the scope of atmospheric science, describes the propagation of radiation through a participating medium: the atmosphere, bounded by the Earth surface. Although many components of the Earth system interact with radiation, clouds play a key role because of their strong impact (globally cooling the Earth) (Ramanathan et al., 1989), their high frequency of occurrence (Rossow & Dues, 2004) and their inherent complexity in both space and time (Davis, Wiscombe, Cahalan, & Marshak, 1994). Radiation and its interactions with clouds are involved in various atmospheric applications at a large range of scales: from the Earth energy balance and cycle relevant to numerical weather predictions (Hogan et al., 2017) and climate studies (Cess et al., 1989; Dufresne & Bony, 2008), to the inhomogeneous heating and cooling rates modifying dynamics and cloud processes at small scales (Klinger, Feingold, & Yamaguchi, 2018; Klinger et al., 2017), and to the retrieval of atmospheric state and properties from radiative quantities such as photon path statistics, spectrally resolved radiances or polarized reflectances (Cornet et al., 2018), observed by both active and passive remote sensors.

In operational contexts, one-dimensional (1D) radiative transfer models are preferred for their simplicity and efficiency. Only very recently has a large-scale parametrization for three-dimensional (3D) effects been developed (Hogan, Schäfer, Klinger, Chiu, & Mayer, 2016; S. A. K. Schäfer, Hogan, Klinger, Chiu, & Mayer, 2016), leading to the very first estimation of the broadband, global, 3D radiative effect of clouds (around 2W/m^2 after S. Schäfer (2016)). This could not have occurred without the long-term efforts of a pioneering group of cloud-radiation scientists, who has been developing and using reference 3D radiative transfer models for the past forty years, to analyze and document cloud-radiation 3D interactions. These 3D models can be divided into two categories:

1. Deterministic methods such as the Spherical Harmonics Discrete Ordinate Method (SHDOM, Evans (1998)) solve a discretized (approximate) version of the radiative transfer equation (RTE): they provide the exact solution to a convergent approximation of the radiative model.
2. Stochastic methods such as the Monte Carlo (MC) techniques (Marchuk, Mikhailov, Nazaratiev, et al., 1980) fundamentally preserve the exact radiative model and provide a convergent statistical estimate of its solution, along with an estimate of its statistical uncertainty (variance).

Monte Carlo methods in particular, because of their ability to evaluate their uncertainty in a quasi-systematic manner, are widely recognized as references in all fields of radiative transfer involving complex geometry and/or high spectral dynamics (Marshak & Davis, 2005). This statement is true beyond atmospheric sciences (Delatorre et al., 2014; Glouchkov, Koshelev, & Schulz, 2003; Spanier & Gelbard, 2008; Veach, 1998). Monte Carlo approaches are powerful tools to solve linear transport models such as the RTE because their solutions are recursive integrals. Since integrals can be regarded as statistical expectations, and since the expectation of another expectation is still only one expectation, the computational cost of solving recursive integrals (a problem of infinite dimension) scales linearly with the recursive depth, instead of exponentially in deterministic methods. In MC algorithms, adding new variables of integration that are not the primary source of variance for the estimated quantity does not increase the computation time needed to reach a given level of convergence. In deterministic methods, a new dimension is added for each variable of integration, rapidly increasing computational cost.

The need for flexible accurate 3D tools able to compute very diverse radiative metrics in user-specified 3D atmospheric fields, including clouds, has long been identified and MC approaches have often been the natural choice. Many codes already exist and some are freely available to the community. It was Collins and Wells (1965) who first applied MC methods to atmospheric radiative transfer, but the extensive work presented in Marchuk, Mikhailov, Nazareliev, et al. (1980) is the pioneering reference. Intercomparison exercises have been organised — the Intercomparison of 3D Radiation Codes (I3RC, Cahalan et al. (2005)) and the International Polarized Radiative Transfer (IPRT, Emde et al. (2015, 2018)) — to document and promote 3D radiative models and bring the community together. Participating MC codes include: Cole (2005); Davies (1978); Kassianov and Kogan (2002); Macke, Mitchell, and Bremen (1999); Marshak, Davis, Wiscombe, and Cahalan (1995); OHirok and Gautier (1998); Takara and Ellingson (1996); Várnai and Marshak (2003), MYSTIC (Mayer & Kylling, 2005), 3DMCPOL (Cornet, Labonnote, & Szczap, 2010; Fauchez, Cornet, Szczap, Dubuisson, & Rosambert, 2014) and SPARTA (Barlakas, Macke, Wendisch, & Ehrlich, 2014), with the last three codes implementing polarization. Other codes exist, such as McArtim (Deutschmann et al., 2011) and McRali (Alkasem et al., 2017; Szczap et al., 2013), oriented towards remote sensing applications; or MCARaTS (Iwabuchi & Kobayashi, 2006), that was coupled with a 3D MC model for surface radiative transfer (Kobayashi & Iwabuchi, 2008) that uses computer graphics techniques to detect ray intersections in complex surfaces such as canopies.

The I3RC exercise led to the development of the *I3RC Community Monte Carlo model* (Pincus & Evans, 2009) in the form of modular tools to compute optical data and solve radiation. A monochromatic shortwave algorithm was implemented with those tools as an illustration of their use. It was recently extended to broadband solar and monochromatic thermal radiation by Jones and Di Girolamo (2018). Indeed, the project was designed as a platform to facilitate the development of atmospheric radiative transfer codes for various applications, that should be completed by the community as needs for new functionalities arise. Much in the lineage of this approach, and with similar intentions, our proposition is the following:

1. benefiting from recent co-developments made by computer scientists and engineering physicists,
2. providing the atmospheric-science community with independent open-source Monte Carlo libraries, to be shared by projects in distinct application contexts.

Developing libraries instead of one code is only possible because abstractions are available ensuring that genericity is preserved when splitting MC codes into algorithmic elements that are interconnected in such a way that their developments can be independent. If this splitting was partly carried out in the I3RC Community code, with abstractions such as *scattering phase functions* or *integrators*, it was notably one of the main tasks of the com-

puter graphics community in the last twenty years, when setting up the algorithmic concepts that led to today's extensive use of MC for rendering images in the cinema industry. Such abstractions are for example *ray-tracing*, based on *rays* (semi-infinite lines defined by their origin and direction); *acceleration structures* for surface intersections, based on *shapes* (basic geometries such as triangles); *bounding boxes* (that divide a volume into subregions); etc. The *Physically Based Rendering* book (3rd edition freely available online, see Pharr and Humphreys (2018)) gives an extensive description of these concepts and examples of their implementation, in a pedagogic literate programming style (Knuth, 1984).

A particularly interesting consequence of this separation is that the data describing the scene (a set of *primitives* of potentially infinite complexity), becomes perfectly independent from the ray-tracing method: algorithms can be optimized in full generality, without constraint about how the geometrical and physical data is structured. Since *integral formulations* are formal equivalents to MC algorithms, they have been a favored tool in optimization tasks: trying to tackle either convergence issues or resource constraints has led the computer graphics scientists to formally modify integral formulations, insuring strict equivalence to the solution and leading to new families of algorithms. For example, the *Bidirectional Path Tracing* (Veach, 1998) was only developed after writing the light transport as an integration problem. It led to a decrease in variance through better sampling of light sources, and in computational effort through a more efficient management of data access since subpaths are reused.

This strategy for designing new algorithms and optimizing them was not initiated by the computer graphics community: radiation physicists have been manipulating integral formulations since the origin of MC simulations. However, in this parallel history of research, both the computer graphics and the radiation physics communities have encountered the same difficulty in handling complex inhomogeneous media: the exponential nature of Beer extension law combines *nonlinearly* the integral over the heterogeneity of the field (integral of the local extinction along the path) to the other radiative transfer integrals (over the scattering directions, wavelengths, etc).

At the origin of the research reported here is a recent major step forward concerning the handling of volumes: it was recently identified that an old MC technique (adding fictitious matter to the medium so as to make it homogeneous, see subsection 2.2) could be seen as an effective way to linearize the integral formulations, i.e. to move the optical depth integral outside the exponential (Dauchet et al., 2018; Eymet et al., 2013; Galtier et al., 2013, 2016). As a result, all the techniques recently developed by the computer graphics community for handling complex surfaces could be reinvested for complex volumes. This application was fast: it was only four years between the formal proposition and its appropriation by the cinema industry to produce new advanced concepts for fast rendering of cloudy scenes (Kutz, Habel, Li, & Novák, 2017; Novák, Georgiev, Hanika, & Jarosz, 2018).

The data–algorithm independence is therefore the root of the present proposition which builds on i/ concept separability, ii/ decades of expertise and developments in the computer graphics community and iii/ bypassing the nonlinearity of Beer's law. The set of libraries we provide should not only allow i/ flexibility in radiative computations as intended by Pincus, Hannay, and Evans (2005), with the possibility to implement any MC algorithm, variance reduction techniques and simultaneous estimate of a metric and its partial derivatives (Dauchet et al., 2013; de Lataillade et al., 2002; Roger, Blanco, Mouna, & Fournier, 2005; Weise & Zhang, 1997), but also ii/ unprecedented performance in the treatment of Earth surface and atmospheric volume complexity, through efficient path-tracing through the data describing it.

In section 2, we review the historical elements that led us to the developments that we later describe in section 4. Before this description we present in section 3 a simple example algorithm that estimates the local direct solar transmissivity. We show how formal manipulation of the equivalent integral formulation can lead to simultaneous computation

of both the transmissivity and its partial derivatives with respect to problem parameters (the Jacobian). In section 5, we illustrate the genericity of these tools by implementing three algorithms related to distinct applications of atmospheric radiative transfer: image synthesis, analysis of transmission under a cloud together with its sensitivity to an optical parameter, and assessment of a parametrization of 3D radiative effects of clouds.

2 Path Tracing in Complex Geometries

In this section, we review the history of *path tracing* inside scenes involving complex surfaces, with a specific attention to the computer science literature devoted to physically-based rendering, which indeed addresses the very same RTE as ours (2.1). We then summarize the recent developments made in the handling of complex volumes by both this community and the engineering physics community (for infrared heat transfer and combustion studies) in 2.2.

2.1 Path tracing and complex surfaces

Image synthesis is the science that aims to numerically produce images from descriptions of scenes. It was born in the 1970s when computer graphics started to expand. At first, the focus was on surface rendering, often assuming the scene objects were surrounded by vacuum. Among the diverse existing techniques, we mention here only a few ones that gradually led to the use of Monte Carlo based path-tracing methods to render 3D scenes. Methods that were dominant in practice (e.g. micropolygon rendering or rasterization) are missing from this text and we refer the interested reader to more complete presentations of the field’s history, e.g. in the section 1.7 of Pharr and Humphreys (2018).

The initial concern was to determine which objects in a scene were visible from a given point of view. Appel (1968) first introduced the *ray casting* method as a general way to solve the *hidden surface problem*, by casting rays from the observer to the scene objects and detecting intersections. This opened a whole field of investigation dedicated to optimizing ray casting, e.g. through efficient intersection tests between rays and large numbers of primary shapes Wald (2004); Wald, Slusallek, Benthin, and Wagner (2001); Wald, Woop, Benthin, Johnson, and Ernst (2014) and references therein).

Once the visible surfaces were found, the next question was to determine how these surfaces were illuminated by the sources and the other surfaces, which was referred to as the *global illumination problem*. Whitted (1980) first used recursive ray casting in the *ray tracing* method, which includes random sampling around optical directions to correct the unrealistically sharp gradients of intensity due to perfectly specular reflections. Cook, Porter, and Carpenter (1984) then generalized the randomly perturbed ray-tracing approach to multi-variate perturbations in the *distributed ray tracing* method. This was the first algorithm able to render all the major realistic visual effects in a unified, coherent way.

A couple of years later, Kajiya (1986) developed the formal framework of the *rendering equation* (the integral formulation of the radiative transfer equation in vacuum, focused on light-surface interactions). His *path tracing* model was the first unbiased scene renderer to be based on MC ray casting. While revisiting this proposition, Arvo and Kirk (1990) found inspiration in the experienced community of particle transport sciences, where MC methods were already commonly used and studied. They introduced variance reduction techniques to the image rendering community.

Another important step towards efficiency was Veach’s pioneering thesis (Veach, 1998). From his mathematical background, he introduced a new paradigm in which radiative quantities were formally expressed as integrals over a *path space*, decoupling the formulation from the underlying physics: the formulations were no longer *analog* (i.e., based on intuitive pictures of the stochastic physics of particle transport). This allowed him to explore sampling

strategies in full generality and to then apply them to path tracing, giving birth to several low-variance algorithms such as the *Bidirectional Path Tracing* (Veach & Guibas, 1995) or the *Metropolis Light Transport* (Veach & Guibas, 1997)

It is only from the years 2000s, with the increase of computing power, that MC physically-based path-tracing techniques were considered viable tools beyond research, for production purposes. They were favored because

1. it was eventually perceived that MC methods allow independence between the rendering algorithm and the description of the scene (i.e. the number and properties of the surfaces to render), thus providing the artists with unprecedented freedom,
2. they allow a unified, physical representation of the interaction of light with surfaces, relieving the artists from the need to arbitrarily modify the surface properties in order to achieve a specific effect, since they could now rely on the physics and
3. improvement of filtering methods have allowed cheap image denoising, thus bypassing the need for more expensive, well-converged MC simulations.

In the recent years, algorithms and techniques have been developed to improve surface rendering performances, either through a reduction of variance or an increase in data management efficiency. Using these same techniques would already be a step forward from our current treatment of ray–surface intersections, in particular when coupling atmospheric radiation to surface radiation in complex grounds, e.g. cities, canopies or mountains. One part of our proposition is to provide the atmospheric community with an implementation of these techniques. The next section is about transposing these tools to radiation–volume interactions.

2.2 Path tracing and complex volumes

A major difficulty in MC methods is the treatment of complex heterogeneities in volumes, in particular in cloudy atmospheres. For decades, the computer graphics handled the question of volumes as have many other MC scientists; their expertise in designing performant ray-casting tools had found its limit in dealing with volume complexity.

The issue resides in the fact that the integral expression of the optical depth, from which is sampled the next collision location, is encapsulated into Beer’s exponential extinction law. This nonlinearity inhibates a powerful feature of MC techniques – sampling multiple integrals: the expectation of a nonlinear function of an expectation is no longer one expectation.

Most commonly, an optical depth is sampled, the extinction is integrated along the photon path to explicitly compute the true optical depth, and the path is stopped whenever the true optical depth equals the sampled optical depth: this is the next collision location. This is called *path tracking* or *regular tracking* and is illustrated in Figure 1 a). This is inherently resolution-dependent since the data contained in each intersected cell of the original grid is accessed to add its contribution to the optical depth. In the context of cloudy atmospheres, a large number of cells with negligible contributions to the optical depth will be crossed, yielding important computational cost since finding intersections and accessing the corresponding data in memory is highly time consuming. Moreover, this method is not able to cope with the fact that the resolution of the data describing complex cloudy atmospheres is vastly increasing: severe expenses will arise as soon as the field stops fitting into the main memory.

A different, unbiased approach appeared under different names in distinct fields. It consists in adding fictitious matter (that has no effect on the transport) in order to reduce the effective resolution of the data, thus decreasing the cost of the grid traversal. This is illustrated in Figure 1 b) where fictitious water droplets have been added to the true cloud layer to make it appear piecewise homogeneous. The optical depth is computed along

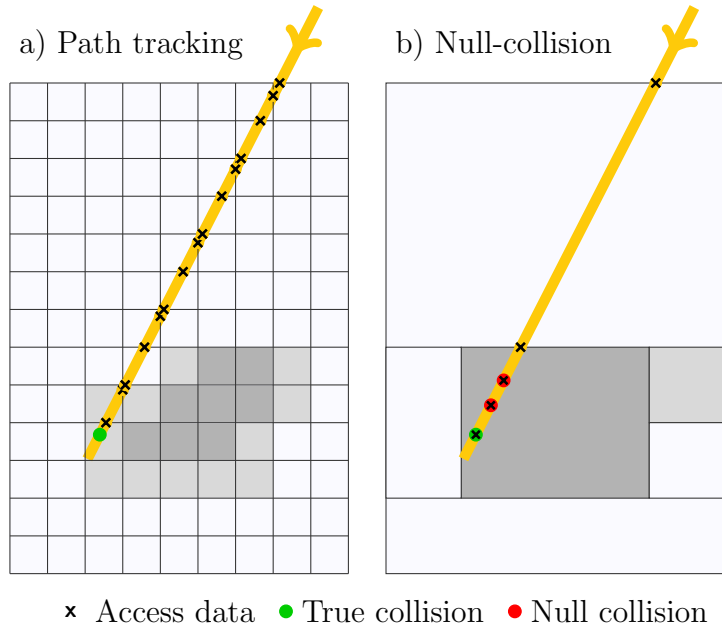


Figure 1. Two unbiased free-path sampling algorithms illustrated on a schematic 2D cloud field. Levels of gray represent the density of colliders in each cell. The thick yellow line represents a ray cast in the field. In both methods, data is accessed in each intersected cell. In *path tracking* (left), the cost of the traversal is fully-dependent on the original data resolution. In *null-collision* (right), coarser effective resolution is achieved by adding fictitious colliders in parts of the domain so as to make it homogeneous-by-parts. The free-paths are sampled from the resulting field with two main consequences: i/ the effective density of colliders is overestimated in some parts of the domain, which is counterbalanced by rejecting some of the sampled collisions (yielding null collisions in red), and ii/ the cost of the traversal is substantially decreased, and no longer depends on the original resolution.

the ray according to the piecewise-uniform (total) extinction coefficient, which leads to an overestimate of collision frequency. At each collision location, the true data is accessed and the collision is either rejected (the first 2 collisions in Figure 1 b)) or accepted (the last collision), based on the random sampling of the local true-to-total extinction ratio.

In neutron transport, this method was first described by Woodcock, Murphy, Hemmings, and Longworth (1965) under the name Woodcock tracking. In plasma simulations it first appeared in Skullerud (1968). Soon after, Coleman (1968) gave a mathematical justification for this method, demonstrating its exactness. In the atmosphere, it was first proposed by Marchuk, Mikhailov, Nazareliev, et al. (1980) and called the *Maximum cross section*. Koura (1986) developed it for rarefied gas under the name null-collisions. Computer graphics have also used it as Woodcock tracking, for the first time in Raab, Seibert, and Keller (2006).

Only with Galtier et al. (2013) seminal paper did it become clear that the expertise of the computer graphics scientists on surface complexity was indeed applicable to volumes. In this paper, null-collision algorithms (NCA) are written as integral formulations, and it is shown that the null-collision methods can be used in a more flexible way, including with negative null-collision extinction coefficients. It is stated that the data–algorithm independence, also strongly highlighted by Eymet et al. (2013), is not a consequence of introducing null-collisions, but rather a consequence of the underlying integral reformulation. This new formulation is presented as a way to bypass Beer’s exponential nonlinearity.

This explicit framework opened doors to new families of MC algorithms, with potential for solving various problems that were before then considered impossible: nonlinear models (Dauchet et al., 2018), coupled radiation-convection-conduction in a single MC algorithm (Fournier, Blanco, Eymet, Mouna, & Spiesser, 2016), energetic state transitions sampled from spectroscopy instead of approximate spectral models (Galtier et al., 2016), symbolic Monte Carlo to scattering media (Galtier, Roger, André, & Delmas, 2017) etc. Some of these methods are transposable to atmospheric radiative transfer with large benefits for our community, e.g. conducto-radiative MC models to investigate atmosphere–cities interactions, or line-sampling methods for benchmark spectral integration, to develop, tune and test spectral models. During the past couple of years, the computer graphics community has been similarly impacted by this new paradigm. Kutz et al. (2017) show how integral formulations of NCA can be used to derive more efficient free-path sampling techniques. Novák et al. (2018) give a good review of the different free-path sampling methods, with a focus on NCA and their newly perceived interest.

In the cloud-radiation community, the maximum cross-section method has often been perceived as a trick. It has been considered inefficient because in the presence of clouds, extinction varies on a large range, and stopping the path to sort out true from null events is time consuming. However, Marshak et al. (1995) highlighted the method’s insensitivity to the number of cells used to describe the medium (i.e. the data–algorithm independence) and Iwabuchi and Kobayashi (2006) was already hinting at optimizations based on the definition of bounded volumes where the total extinction would be constant, leading to a piecewise-uniform extinction field. This comes back to partitioning data into accelerating structures that could be efficiently crossed, which is at the heart of the computer graphics expertise when dealing with surfaces. Our core contribution consists in transposing this expertise to volumes.

3 Integral Formulations of Null-Collision Monte Carlo Algorithms

Most of the work mentioned in the last section is based on integral formulations manipulations. They are powerful tools to improve Monte Carlo algorithms as they offer a formal framework to derive non-analog equivalents, that can then be translated into new algorithms

(Dauchet et al., 2013; Delatorre et al., 2014; Eymet, Fournier, Blanco, & Dufresne, 2005). In this section, we first show how a simple algorithm translates into its integral formulation.

As an illustration, we present an algorithm that computes the direct (unscattered) solar transmissivity T of the cloudy atmosphere, at a location \mathbf{x}_0 . The sun illuminates the top of the atmosphere (TOA) uniformly and is directed along ω . The only surfaces in the scene are a set of opaque triangles that describe the orography. The original data for the atmosphere is a meshed field of extinction coefficients k .

The backward null-collision algorithm presented here implements the variance-reduction *decomposition tracking* technique (Kutz et al., 2017; Novák, Selle, & Jarosz, 2014): the medium is decomposed into a *control* homogeneous medium where the value of direct transmissivity is analytically computed, and a *residual* medium that is associated to the heterogeneities, where the direct transmissivity is evaluated through MC sampling. The paths are traced from \mathbf{x}_0 to the sun in the direction ω .

Preliminary steps consist in building acceleration structures for the surface and for the volume. For the volume, the cells that constitute the original grid are tested for merging against a criterium that will be discussed in section 5. In each "super-cell", or voxel, \mathcal{V}_i of the acceleration structure, minimum and maximum extinction coefficients are computed and saved: $k_{i,min} = \min \{k(\mathbf{x}), \forall \mathbf{x} \in \mathcal{V}_i\}$, $k_{i,max} = \max \{k(\mathbf{x}), \forall \mathbf{x} \in \mathcal{V}_i\}$.

The steps to compute one realization t of the random variable T are the following:

1. Cast a ray in the scene, originating from \mathbf{x}_0 in the direction ω , until the first opaque surface is intersected. The procedure for intersection with orography is typical of computer graphics when only surfaces are considered, as if the volume was empty.
2. If a surface is intersected, return $t = 0$; the only surfaces in the scene are opaque, and we are looking at the *direct* solar transmissivity thus if a hit is found, there is no transmission.
3. If no surface is intersected, sample a free-path τ_s .
4. Trace a ray in the volume, originating from \mathbf{x}_0 in the direction ω , and find the first collision. At this stage, only the acceleration structure is visited and the collisions that are looked at correspond to the overestimate of the residual extinction coefficient within each voxel \mathcal{V}_i : $\forall \mathbf{x} \in \mathcal{V}_i, \hat{k}(\mathbf{x}) \equiv k_{i,max} - k_{i,min}$
5. If no collision is found before the TOA, return $t = \exp(-\sum_i k_{i,min} l_i)$ where l_i is the length of the intersection of the ray with \mathcal{V}_i . As no collision was detected in the field of the overestimate residual extinction coefficient, no collision would occur in the true residual field; the transmission is complete and the transmissivity of the control medium is returned.
6. If a collision is detected at location $\mathbf{x}_s \in \mathcal{V}_i$, access the true extinction coefficient $k(\mathbf{x}_s)$, compute the residual coefficient $k_r(\mathbf{x}_s) = k(\mathbf{x}_s) - k_{i,min}$, and the probability of true collision $P(\mathbf{x}_s) = \frac{k_r(\mathbf{x}_s)}{\hat{k}(\mathbf{x}_s)}$.
7. Sample a random number ϵ uniformly in $[0, 1[$ in order to decide between a true and a null collision.
8. If $\epsilon < P(\mathbf{x}_s)$, return $t = 0$. A true collision occurred and there is no transmission.
9. Otherwise, set \mathbf{x}_0 to \mathbf{x} and loop to step 3.

The resulting algorithm is strictly equivalent to the following integral formulation:

$$\begin{aligned}
 T(\mathbf{x}_0, \omega) = & \int_0^\infty d\hat{\tau}_s \overbrace{\exp(-\hat{\tau}_s)}^{3.} \left(\overbrace{H(\hat{\tau}_s - \hat{\tau}_L) \{ \exp(-\tau_{min}) \}}^{5.} \right. \\
 & \left. + \overbrace{H(\hat{\tau}_L - \hat{\tau}_s)}^{6.} \left(\underbrace{\frac{k_r(\mathbf{x}_s)}{\hat{k}(\mathbf{x}_s)}}_{8.} \{0\} + \underbrace{\left(1 - \frac{k_r(\mathbf{x}_s)}{\hat{k}(\mathbf{x}_s)}\right)}_{9.} \{T(\mathbf{x}_s, \omega)\} \right) \right) \quad (1)
 \end{aligned}$$

where for any positive distance s , $\hat{\tau}_s = \int_0^s \hat{k}(\mathbf{x}_1) l dl$ is the overestimate of the residual optical depth between \mathbf{x} and $\mathbf{x}_s = \mathbf{x}_0 + \omega s$. L is the distance to TOA along ω , $\tau_{min} = \int_0^L k_{min}(\mathbf{x}_1) l dl$ is the control optical depth from \mathbf{x} to \mathbf{x}_L , and H is the Heaviside function. Braces indicate correspondance with the steps described above to highlight the equivalence between the formulation and the algorithm.

In general, integrals represent samplings and the integrands are a combination of probability density functions (pdfs) from which random variables are sampled, deterministic tests (H) and MC weights (into brackets). Ratios can be interpreted as discrete probabilities (i.e. random tests) or contribute to the MC weights. This strict correspondance between algorithm and integral formulation is very useful when designing optimizations for algorithms that poorly estimate a quantity, either because the variance is too high, or the computing performance too low. It provides a formal framework, that we use in the following to derive an algorithm that simultaneously computes the direct transmissivity and its partial derivatives.

Indeed, it is always possible to write, from the integral formulation of a MC algorithm, a derived formulation that conserves the pdfs of the original formulation (de Lataillade et al., 2002; Mikhailov & Sabelfeld, 1995; Roger et al., 2005). The derivations are affected to the MC weights instead of the pdfs: the same randomly-sampled paths are used to estimate the quantity and its partial derivatives. This means the same simulation can be used to simultaneously estimate the quantity and its derivatives with respect to any number of model parameters. This is in particular useful to assess the sensitivity of radiative metrics to uncertain optical parameters, with implications for data assimilation, atmospheric state retrievals, and analysis of the 3D interactions between radiation and atmospheric or surface properties.

The first step is to derive the integral formulation (1) with respect to the parameter of interest, Π . In theory, any pdf or weight expression can depend on the parameter of derivation. Here, only the true field of extinction coefficients, k , depends on Π :

$$\begin{aligned} \partial_{\Pi} T(\mathbf{x}_0) &= \int_0^{\infty} d\hat{\tau}_s \exp(-\hat{\tau}_s) \left(H(\hat{\tau}_s - \hat{\tau}_L) \{0\} + H(\hat{\tau}_L - \hat{\tau}_s) \right. \\ &\quad \left. \times \left(\frac{\partial_{\Pi} k_r(\mathbf{x}_s)}{\hat{k}(\mathbf{x}_s)} \{0\} - \frac{\partial_{\Pi} k_r(\mathbf{x}_s)}{\hat{k}(\mathbf{x}_s)} \{T(\mathbf{x}_s)\} + \left(1 - \frac{k_r(\mathbf{x}_s)}{\hat{k}(\mathbf{x}_s)}\right) \{\partial_{\Pi} T(\mathbf{x}_s)\} \right) \right) \end{aligned} \quad (2)$$

Then, we transform the formulation (2) so as to retrieve the pdfs that were sampled in the direct transmissivity algorithm (1):

$$\begin{aligned} \partial_{\Pi} T(\mathbf{x}_0) &= \int_0^{\infty} d\hat{\tau}_s \exp(-\hat{\tau}_s) \left(H(\hat{\tau}_s - \hat{\tau}_L) \{0\} + H(\hat{\tau}_L - \hat{\tau}_s) \right. \\ &\quad \left. \times \left(\frac{k_r(\mathbf{x}_s)}{\hat{k}(\mathbf{x}_s)} \{0\} + \left(1 - \frac{k_r(\mathbf{x}_s)}{\hat{k}(\mathbf{x}_s)}\right) \left\{ -\frac{\partial_{\Pi} k_r(\mathbf{x}_s)}{\hat{k}(\mathbf{x}_s) - k_r(\mathbf{x}_s)} T(\mathbf{x}_s) + \partial_{\Pi} T(\mathbf{x}_s) \right\} \right) \right) \end{aligned} \quad (3)$$

The only difference between formulations (1) and (3) are the MC weights. In particular, the sensitivity weight in case of null-collision is the sum of two contributions: i/ the sensitivity of the null-collision probability to the parameter and ii/ the sensitivity of the transmissivity itself. Since the pdfs haven't changed, we can use the same random paths (i.e. the same sequences of free-paths and collisions nature) to simultaneously estimate the direct transmissivity and its derivatives with respect to one or many parameters Π , by updating a different counter for each metric. This is possible as long as we can evaluate $\partial_{\Pi} k_r(\mathbf{x})$ for all \mathbf{x} in the domain, which may not be trivial. For example, new integrals might appear in the derivative formulation and additional random sampling might be necessary to estimate them, thus slightly increasing the cost of the global computation. Another matter is that the convergence of the derivatives estimate is seldom as fast as the convergence of the metric estimate, in particular when trying to estimate weak sensitivities, as illustrated in subsection 5.2.

4 Implementation of Libraries and Data Production

If the previous sections we discussed the literature and the conceptual developments that led us to the present proposition. This section and the next introduce and discuss our contribution. We start by briefly describing the main modules that have been implemented as elementary and independent libraries to facilitate the development of short readable codes (4.1). To complete the chain of tools, we expose the main choices underlying the production of the optical properties we use for gas (4.2) and clouds (4.3).

Apart from the idea of embedding 3D fields into stratified 1D vertical profiles, nothing in the described libraries depends on the type and structure of the data: we could treat any type of cloud, aerosol or gas as long as their distribution in the atmosphere and their optical properties are provided. This is a strength as far as development is concerned, but it does not reduce the very significant efforts required to produce and interface the data, in particular for the spectral dependence of gaseous absorption.

4.1 Building blocks for Monte Carlo development

The modules are briefly presented in Table 1 and divided into three groups:

1. low-level modules (random sampling, ray-tracing, scattering), implemented as libraries, available in the Star-Engine (SE, <https://gitlab.com/meso-star/star-engine/>) environment. They implement true abstractions of Monte Carlo concepts that can be used regardless of the scientific field of application;
2. data-oriented modules (3D atmospheric fields, cloud and gas optical properties data), also implemented as libraries although not available in the SE environment since already oriented towards atmospheric applications;
3. application-oriented modules (sky, ground, camera and sun), not implemented as libraries, developed in the context of the renderer application. They can be used for other projects implementing atmospheric radiative transfer models.

Typical functions associated to the different modules are cited as illustrations. The sources can be downloaded online (<https://www.meso-star.com/projects/high-tune/high-tune.html>) and user-guides are provided on the website. A starter-pack is also provided with the data and scripts necessary to reproduce the examples of section 5.

However, the most useful user-guide for the interested reader is the commented code that implements the algorithm described in 5.1, using the various functions of Table 1. Indeed, this code was in part developed to illustrate the use of the different libraries and modules, to serve as a basis for further developments, or as an example to implement new algorithms.

To test these tools in the context of multiple scattering, we implemented several benchmark experiments and compared our calculations against published results, e.g. Table 1 of Galtier et al. (2013), or against the solution of the well-validated 3DMCPOL (Cornet et al., 2010) on the IPRT cubic cloud case (Emde et al., 2018) (see Supporting Information). Agreement was found within the MC statistical uncertainty, thus validating our implementations.

4.2 Clear sky data

The radiative properties of the gas mixture are those of the Rapid Radiative Transfer Model for GCMs (RRTMG, Iacono et al. (2008); Mlawer, Taubman, Brown, Iacono, and Clough (1997)). We access them via the ecRad radiative transfer model developed at the ECMWF (Hogan & Bozzo, 2018), that we use as a front-end for production of k-distributions (Fu & Liou, 1992) for 16 spectral intervals in the longwave (LW) region ($[10-3500]$ cm^{-1}) and 14 spectral intervals in the shortwave (SW) ($[820-50000]$ cm^{-1}). Each quadrature

Table 1. Open-source Monte Carlo modules and examples of functions. The list of functions is not comprehensive. Most of the functions mentioned here can be found in the commented implementation of the renderer presented in 5.1, which source code is available at <https://gitlab.com/meso-star/htrdr>.

Module name	Description	Example of functions
Low-level (Star-Engine)	https://gitlab.com/meso-star/star-engine/	
Star-Sample (ssp)	Generate reproducible sequences of pseudo-random numbers (compatible with parallelization), sample and evaluate various probability density functions.	ssp_rng_canonical; ssp_ran_exp_pdf; ssp_ran_hemisphere_cos;
Star-3D (s3d)	Define shapes, attach them to a scene, trace rays in the scene, filter hits.	s3d_scene_create; s3d_scene_view_trace_ray; s3d_hit_filter_function_T;
Star-Voxel (svx)	Define voxels, partition them into a hierarchical structure (tree), trace rays in the tree, filter hits.	svx_octree_create; svx_tree_trace_ray; svx_hit_filter_T;
Star-ScatteringFunctions (ssf)	Setup, sample and evaluate scattering functions for surface and volume.	ssf_specular_reflection_setup; ssf_phase_sample; ssf_fresnel_eval;
Data-oriented (High-Tune)	https://www.meso-star.com/projects/high-tune/high-tune.html	
High-Tune: Cloud properties (htcp)	Describe 4D atmospheric fields.	les2htcp (bin)
High-Tune: Mie (htmie)	Describe the optical properties of water droplets.	htmie_fetch_xsection_scattering; htmie_compute_xsection_absorption_average;
High-Tune: Gas Optical properties (htgop)	Describe the optical properties of atmospheric gas mixture.	htgop_get_sw_spectral_interval; htgop_layer_lw_spectral_interval_tab_fetch_ka;
Application-oriented (High-Tune: Renderer)	https://www.meso-star.com/projects/high-tune/high-tune.html	
htrdr_sky	Build acceleration grid for the atmospheric volume data (3D clouds embedded in 1D gas) in the context of null-collision algorithms, trace rays in the atmospheric volume, access null-collision and raw data.	htrdr_sky_create; htrdr_sky_fetch_raw_property; htrdr_sky_fetch_svx_property; htrdr_sky_trace_ray;
htrdr_ground	Build scene and acceleration structure from input obj file describing the ground as a set of triangles, trace rays in the scene.	htrdr_ground_create; htrdr_ground_trace_ray;
htrdr_sun	Implement a sun model, sample solar cone, access sun data.	htrdr_sun_create; htrdr_sun_sample_direction; htrdr_sun_get_radiance;
htrdr_camera	Implement a pinpoint camera model, trace a ray originating from the camera lens.	htrdr_camera_create; htrdr_camera_ray;

point, in each spectral interval, is provided with a quadrature weight that is used by our algorithms as a probability for the sampling of absorption coefficient values that are then practically used as if radiative transfer was monochromatic. The only subtlety is related to the variability of the water vapor concentration in the 3D domain. The water vapor mixing ratio, temperature and pressure are provided in each cell of the 3D domain. We could easily show that the impact of the horizontal variations of temperature and pressure on the absorption was negligible, which led us to only consider the vertical profiles of horizontally-averaged temperature and pressure fields. For water vapor, we used the fact that the absorption coefficient of the gas mixture is roughly linear (in log/log space) with x_{H_2O} , the water vapor molar fraction, except for very small and very high values of x_{H_2O} . The ecRad software was therefore used in a preliminary step to compute absorption and scattering coefficients for the 1D atmosphere, for every LW and SW interval and every quadrature point in every atmospheric layer, for a given discretized range of the water vapor molar fraction x_{H_2O} . The resulting look-up table is then used within the MC algorithm to rapidly retrieve the local k-values. Details describing the model and the interpolation procedure are given in the Supporting Information, along with a plot of the relative error on LW net fluxes. The maximum relative error between two profiles computed analytically from RRTM-G vs. interpolated absorption coefficients is around 1.2%. This is around half the maximum relative error found between profiles computed by ecRad vs. analytically, from RRTM-G data (2.6%).

4.3 Cloud data

Mishchenko, D. Travis, and Lacis (2002) is used to solve far-field light scattering by spherical particles using the Lorenz-Mie theory. The main hypothesis are that the droplets are homogeneous and polarization is ignored. As with ecRad for gaseous absorption, this code is used externally to compute the single scattering albedo, the extinction coefficient (along with scattering and absorption coefficients), the asymmetry parameter and the phase function, all of these properties being averaged over the size distribution. We also compute the cumulative phase function and its inverse to allow efficient sampling of scattering directions. The MC algorithm accesses these data via look-up tables. The particular table that was used for the simulations of section 5 is available as a NetCDF file in the starter-pack (<https://www.meso-star.com/projects/high-tune/starter-pack.html>).

5 Examples of Monte Carlo Codes Implementing the Libraries

To illustrate the variety of MC codes that can be implemented from the modules we provide, we present three different MC algorithms that simulate the propagation of radiation in cumulus and stratocumulus fields. The cloud fields are outputs from Large Eddy Simulations of the standard ARM-Cumulus (Brown et al. (2002), hereafter ARMCu), BOMEX (Siebesma et al. (2003), but with a larger domain of $12.8 \times 12.8 \text{ km}^2$) and FIRE (Duykerke et al., 2004), run with the non-hydrostatic model MesoNH (Lac et al., 2018) at a resolution of 25m (ARMCu and BOMEX) to 50m (FIRE). We consider optical properties to be homogeneous in each grid. Since the one-moment microphysical scheme used in the simulations only provides a liquid water mixing ratio, we arbitrarily assume a constant droplet size distribution shaped as a lognormal of mean $10 \mu\text{m}$ and standard deviation $1 \mu\text{m}$. The asymmetry parameter g is taken from Mie computations but in order to avoid convergence issues in reverse MC, we use the approximate Henyey-Greenstein (HG) phase function as the cloud droplets scattering phase function instead of the true Mie phase function. Available algorithms using unbiased variance reduction techniques to handle the Mie phase function have not been implemented yet (Buras & Mayer, 2011; Iwabuchi, 2006).

The first example is an image renderer in the visible part of the spectrum, that generates unbiased synthetic images of clouds and topology. We discuss computing performances related to the use of the libraries. In the second illustration, we estimate the solar

monochromatic transmissivity of cloudy atmosphere at the surface, along with its derivative with respect to the absorption-to-extinction ratio, using the same technique as described in section 3. The third algorithm is broadband solar forward with the true Mie phase function and estimates the horizontally averaged direct and diffuse components of the incident flux at the surface for evaluation of a parametrization. We discuss the importance of representing 3D effects.

5.1 Rendering LES cloud images

Here we accurately simulate synthetic images that are true radiative quantities: exact radiances spectrally integrated over three typical sensors (the spectral response functions) of human vision. This allows 3D visualization of atmospheric data which helps judging the realism of LES simulations, but also provides information on the 3D paths of light and their complex interactions with clouds. It is also helpful to evaluate inverse models, since we can compare resolved 3D fields that are used to synthesize radiative observations, to retrievals generated by inverse models inputted with this same synthetic observations. Rendering accurate high-quality images with MC techniques is challenging since many samples per pixel are needed to reach convergence. Computational effort can quickly become impracticable.

Here we implement a backward MC algorithm. The sun is seen under a given solid angle and illuminates the TOA uniformly. No truly advanced technique for variance reduction has been implemented at this stage. Figure 2 provides image examples of typical cloudy scenes produced using this algorithm. All the images were produced using a laptop with 32GB of random access memory, on an Intel(R) CPU clocked at 2.6GHz.

The radiative paths are initiated at the camera and are followed backward along multiple scattering, multiple reflection trajectories that end either when reaching the TOA, or when absorption occurs. At each scattering and reflection event, the contribution of the direct sun is estimated as described in 3 and added to the path-weight, following the local estimate method (Marchuk, Mikhailov, Nazareliev, et al., 1980). The signal received by the camera is then evaluated as the average value of the path-weights of each MC realization.

5.1.1 Acceleration structures for surfaces

An acceleration structure for surfaces is built as a preliminary step to the rendering algorithm. This is achieved through the Star-3D library, that directly uses the state-of-the-art Embree *application programming interface* (Wald et al., 2014). It partitions and sorts the scene elementary shapes into bounding boxes to reduce the number of intersection tests when a ray is traced. When the ray crosses a bounding box, it only tests the intersections with the shapes within it and all the acceleration comes from the way this structure is refined as a function of the shapes density: too much refinement implies that time is spent crossing a large number of bounding boxes; not enough refinement implies that many triangles need to be tested in each one. This now very typical acceleration procedure changes nothing to the final result but only reduces the time spent accessing and testing geometrical data. In practice this means that the time required to produce the images of Figure 2 is nearly insensitive to the degree of details used to represent the ground, as illustrated in Figure 3-left.

5.1.2 Acceleration structures for volumes

The very same idea is applied to complex volumes: we use an acceleration structure that changes nothing to the result but reduces the computation time. Cells from the original grid are merged together to reduce the number of voxels to cross when looking for the next collision location. The resulting voxels are then hierarchized into octrees (for 3D fields) or binary trees (for 1D fields) to accelerate the crossing. The structure is refined as a function of collision density (based on a residual optical depth criterium). Figure 3-top-



Figure 2. Rendering of LES fields from the BOMEX (upper left), ARMCu (upper right and lower left) and FIRE (lower right) cases. Camera configurations and sun positions are the same as in the scenes from the starter-pack, available online. The definition is 1280x720 pixels, with 2048 samples per pixel component (and 3 components per pixel). Computing times for the same scenes but with 512x512 pixels and 64 samples per pixel component ($512 \times 512 \times 64 \times 3 = 50,331,648$ paths in total) are, from top left to bottom right: 9min, 26min, 11min, 41min. Computing time increases linearly with the number of total paths.

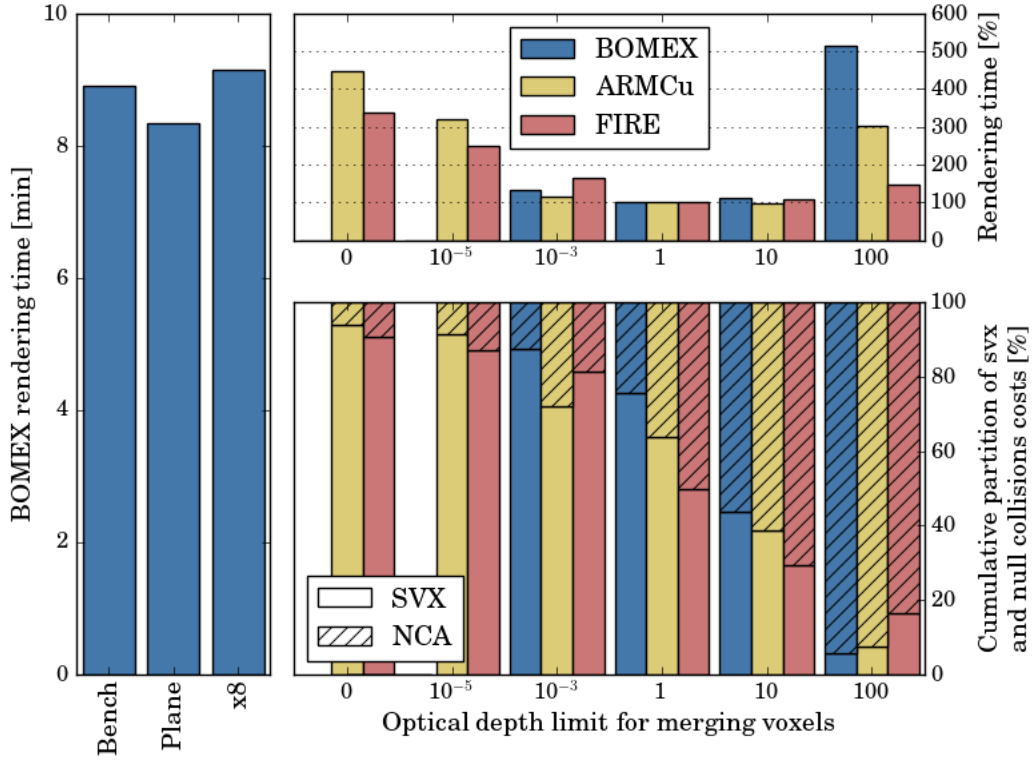


Figure 3. Performance analysis, including acceleration procedures and out of core calculations, on scenes with resolution 512x512 pixels and 64 samples per pixel. Left: rendering time for the original BOMEX scene and two variants, with a plane ground (2 triangles instead of 8,388,608) and with artificially doubled resolution in all three dimensions (8 times more voxels in the raw data grid). Right: dependence of computing time and its partition into i/ crossing and accessing acceleration structure voxels (SVX) vs ii/ accessing raw data and testing collision nature (NCA), to the maximum residual optical depth of the merged voxels. Small values for this limit correspond to refined structures. Note that BOMEX values are missing for maximum residual optical depths $\leq 10^{-5}$ because the acceleration structures (one per quadrature point) did not fit into the main memory (the BOMEX fields are 4 times larger than the ARMCu fields).

right indicates that for the tested algorithm, a maximum residual optical depth of 1 is close to an optimum for all the tested scenes: one collision occurs in average in each voxel. Looking at the partitioning into i/ crossing and accessing acceleration structure voxels (SVX) vs ii/ accessing raw data and testing collision nature (NCA), Figure 3-bottom-right shows that too much refinement implies that time is spent crossing a large number of voxels; not enough refinement implies that the null-collision extinction coefficient can be large in most parts of the voxel, yielding many rejected collisions. As expected the optimum is between the limits of systematically crossing each cell of the original LES data, and using the brute force maximum cross-section approach.

5.1.3 Handling large amounts of data

One further feature of the libraries ought to be highlighted: the `htcp` module that handles the LES fields partitions the raw data in such a way that out of core calculations are affordable. If we think of high resolution LES fields that would not fit into the main memory, a solution is to store them on the disk and load them into the memory only when required. Optimizations of disk access and memory loading are implemented in `htcp` to handle this limit. Figure 3-left illustrates the weak sensitivity of computation time to the size of the LES data, that was artificially increased by a factor 8 for comparison. These features are not yet implemented in `Star-Voxel` and `Star-3D`, i.e. the acceleration structures cannot be *out of core*: no computation can be performed if they do not fit into the main memory. However, acceleration structures are usually much lighter than raw data, and they have the advantage of being adaptative: decreasing the degree of refinement of the structures leads to smaller amounts of data that can eventually fit into the main memory, as was the case for the BOMEX scene.

5.2 Parametric sensitivities

Interactions between clouds and radiation involve many uncertain parameters that impact the metrics in complex, non-linear ways. The sensitivities to these parameters i.e. their partial derivatives, carry rich information useful for analysis as well as in the context of inversion and assimilation of observations (Deutschmann et al., 2011; Marchuk, Mikhailov, Nazareliev, et al., 1980). Here, we implement a backward MC algorithm to estimate local hemispheric monochromatic transmissivity. Atmospheric optical depth is set to zero, only clouds interact with radiation. The sun, directed along a given direction, illuminates the TOA uniformly. With a few extra code lines, we implement the simultaneous computation of the transmissivity sensitivity to the absorptivity of cloud droplets, α (the ratio of absorption over extinction coefficients). This parameter is an output of Mie computations, that rely on hypothesis such as droplet size distribution and purity. Results of a simulation in an ARMCu field with the sun at the zenith is shown in Figure 4.

Evidences of 3D effects appear in Figure 4: transmissivity in clear sky is greater than 1 near the clouds due to sideways leakage of photons through cloud edges. The transmissivity sensitivity to the absorption ratio is negative since more absorption compensated by less scattering yields less total transmissivity, with a maximum under the cloud and slow return to zero elsewhere. The fact that this sensitivity is non-zero under clear sky conditions is another evidence of the remote horizontal influence of clouds on local radiation.

Since algorithms are in general optimized to produce a low variance on the quantity estimate, there is no guarantee that the variance of the derivative estimate will also be low. We see in Figure 4 that the three standard deviations interval ($\pm 3\sigma$, represented as a shaded area around the curves) is much more important around the sensitivity than around the quantity itself. This is due to known difficulties associated to the computation of sensitivities in highly scattering medium. Investigations to efficiently reduce this variance without losing convergence on the quantity itself is currently undergoing.

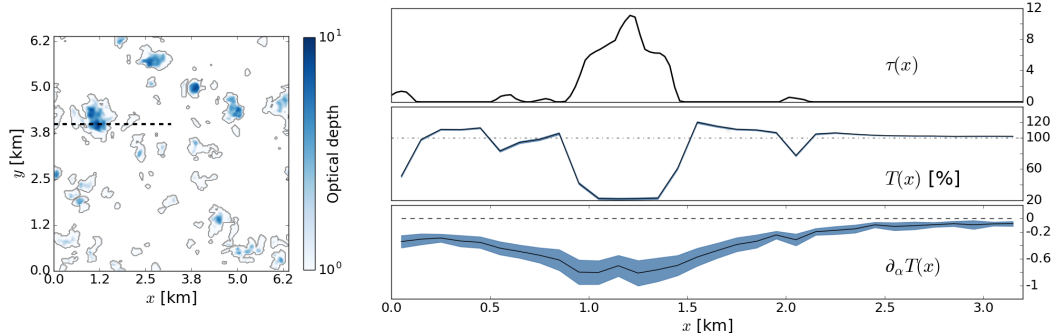


Figure 4. Left: ARMCu 6th hour cloud field (1330 Local Time), logarithmic shade of optical depth. Right: optical depth τ , transmissivity T and its sensitivity to the absorption-to-extinction ratio along the dashed line shown on the left figure. Blue shaded areas represent the 3σ confidence interval estimated by Monte Carlo. The estimation of the transmissivity and its derivative was achieved without approximation, through a unique MC computation.

5.3 Evaluation of a large-scale radiative transfer parametrization

In large-scale models, no detailed information is available to describe the sub-grid atmosphere. In most radiative schemes, the representation of the medium is simplified and 1D solvers that neglect the horizontal transport of light are preferred to more expensive 3D solvers. These are demonstrably poor approximations in cloudy conditions (Barker, Cole, Li, Yi, & Yang, 2015; Barker et al., 2003), particularly in broken cloud fields where clouds highly vary at microscopic and macroscopic scales and cloud edges play an important role in the radiative fluxes distribution and divergence as they materialize a large portion of the interface between cloudy- and clear-sky (Benner & Evans, 2001; Davies, 1978; Harshvardhan, Weinman, & Davies, 1981; Hinkelman, Evans, Clothiaux, Ackerman, & Stackhouse, 2007; Kato & Marshak, 2009; McKee & Klehr, 1978; Pincus et al., 2005).

Possible solver choices implemented in the flexible radiation scheme ecRad (Hogan & Bozzo, 2018) include Tripleclouds, a 1D two-stream solver that represents subgrid horizontal variability of the medium by defining three regions in each layer (Shonk & Hogan, 2008) and the SPARTACUS solver (Hogan et al., 2016; S. A. K. Schäfer et al., 2016) based on Tripleclouds but that additionally represents the effect of horizontal transport on the vertical fluxes. We describe here MC calculations in an ARMCu field that is used as a reference to evaluate ecRad and its parametrization of 3D effects. The assessment is based on the direct-to-total fluxes ratio at the surface.

In the broadband solar forward MC, direct and diffuse fluxes are horizontally integrated: photons contribute to the same estimate independently of their horizontal location when they hit the surface. A photon contributes to the diffuse flux if it has been scattered at least once. However, a limitation resides in the difficulty to reach a consensus to define direct radiation. In solvers based on the two-stream model such as Tripleclouds and SPARTACUS, using true optical parameters leads to an underestimation of transmissivity due to diffuse radiation virtually travelling along two slantwise directions, when in reality, clouds scatter a large amount of radiation in a very small solid angle around the forward direction.

The delta-Eddington scaling technique (Joseph, Wiscombe, & Weinman, 1976) is generally applied to correct for the too reflective clouds: the optical depth and asymmetry parameter are reduced to artificially avoid the scattering of some of the forward scattered photons, leading to an overestimation of direct radiation. To represent this uncertainty in the evaluation, two MC computations are shown: using the true Mie phase function or a

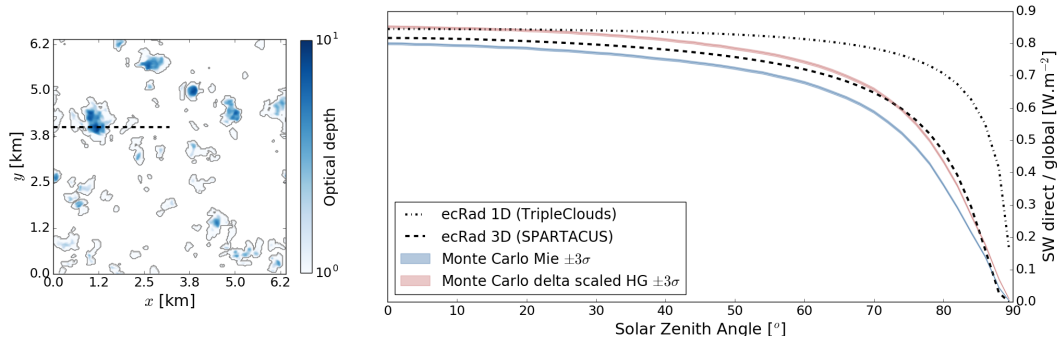


Figure 5. Left: ARMCu 8th hour cloud field (1530 Local Time), logarithmic shade of optical depth. Right: Monte Carlo vs. ecRad computations of surface horizontally averaged direct-to-total fluxes ratio, as a function of solar zenith angle. Results from two ecRad simulations with different solvers (Tripleclouds and SPARTACUS) are plotted to evidence the impact of 3D effects on the partition of surfaces fluxes. Results from two MC simulations with different phase functions (Mie or delta-Eddington scaled Henyey-Greenstein) are plotted to represent uncertainty on the definition of direct and diffuse radiation.

delta-Eddington scaled HG phase function. Periodic conditions are imposed at the walls around the LES domain. Relevant cloud parameters such as overlap and cloud sizes are diagnosed in the LES field and fed to ecRad. The cloud field optical depth and results are shown in Figure 5.

The evolution of the direct-to-total fluxes ratio at the surface is plotted as a function of the solar zenith angle. Since the effective cover increases when the sun is lower in the sky, more of the direct beam is intercepted by clouds through their edges. Without 3D effects, ecRad fails to represent the evolution of the ratio with respect to the solar zenith angle. Good agreement is found between MC and ecRad when these 3D effects are represented i.e. when the SPARTACUS solver is used, effectively reducing the amount of direct radiation at large solar zenith angles.

6 Conclusions

Motivated by needs of flexibility and orthogonality (that we define as the the algorithm being independant of the structure and complexity of the data), we propose a library-based framework for developing Monte Carlo codes for atmospheric radiative transfer. We provide the community of radiative transfer specialists with independent libraries that implement abstract concepts and state-of-the-art ray-tracing techniques that can be used in any MC code, even outside atmospheric sciences (the very same tools are presently used to simulate radiative transfer in combustion LES fields).

Since our work is anchored in a diversity of scientific fields, our proposition is transverse and enriched with concepts that are not fundamentally new but that other communities have brought to a level of maturity that we think will benefit the atmospheric sciences. Such concepts are for example ray casting techniques in surfaces and volumes from the computer graphics community, null-collision algorithms and their potential in efficiently tracing paths in complex heterogeneous media, and derivation of integral formulations to simultaneously compute a quantity and its sensitivities to model parameters.

We illustrate concrete use of our tools on examples that implement above-mentioned concepts and techniques:

1. First, a renderer produces synthetic images of clouds and topography (built as spectrally integrated radiances), simulating the response of sensors detecting radiation in the visible part of the spectrum, for any sun and camera position or direction. With the same tools, we could have developed a similar algorithm to render monochromatic, microwave or infrared images of the atmosphere. We show that the computing time is insensitive to the complexity of both surface and volume and to the amount of data describing them, thanks to acceleration structures and null-collision algorithms. Using a maximum residual optical depth of 1 as a criterium to merge voxels when building the volume acceleration structure leads to an optimal balance between voxel crossing and null-collision sampling. With this optimum, using null-collisions instead of regular tracking accelerates computation by a factor of 3.5 to 4.5 (and probably even more for higher resolution LES fields). The code implementing this example, available at <https://gitlab.com/meso-star/htrdr>, is well-commented and is intended to serve as a guideline for using our libraries.
2. In our second illustration, we focus on integral formulation manipulations. We first derive then rearrange an integral formulation so that the resulting algorithm simultaneously computes the metric and its derivatives with respect to model parameters. If nothing insures that the derivatives will converge as fast as the metric itself, the interesting point is that the derivatives are computed at almost no extra cost since they reuse the same path samples. However, ongoing investigations aim to improve convergence of derivatives (which is knowingly slow in media where scattering dominates absorption).
3. Our third example illustrates the use of our tools in the context of evaluating model-parametrizations. In particular we show that the direct / diffuse partition of fluxes is sensitive to whether 3D radiative effects are taken into account, and to the definition of the direct flux. In the broad context of parametrization and in the continuity of existing studies, these tools could also be used to figure out which mechanisms are key for radiative transfer, to support the development of new features in radiative schemes, or to produce benchmark results to feed tuning tools or statistic models such as neural networks.

We did not compare our codes performance to other existing codes in the literature. Indeed, our efforts were directed towards computing performance rather than fast algorithmic convergence, whereas the true efficiency of MC codes relies on both these aspects. Here, our computing speed is still limited by the time needed to treat the input volume data: embedding 3D fields into 1D profiles and computing the resulting extinction coefficient field is numerically expensive, in particular when handling large amounts of data. But this is related to the application rather than to the libraries themselves.

Regarding the libraries, we can expect some improvement in the future, in particular with respect to the treatment of volume partitionning. Indeed, if structures such as bounding volumes hierarchies are standard for surface acceleration, no similar consensus has been reached for volumes yet, and many options remain that are worth exploring.

Further improvement can be reached by reconsidering the treatment of the spectral dimension. Here, we have built one acceleration structure for each quadrature point of our spectral model, but this would be impracticable with high resolution spectrums. Other partitionning strategies might prove more efficient even for small amounts of spectral data. Another point related to volume data partitionning is the criterium for merging cells. Here, we chose a physically-based criterium but more work would be needed to challenge this arbitrary choice. This point was also raised by the computer graphics community (Yue, Iwasaki, Chen, Dobashi, & Nishita, 2011) and is currently under investigation.

Finally, algorithmic developments can also be undertaken to improve the convergence of the estimators described here: existing or new solutions can be implemented and the question of the partial derivatives convergence further investigated. If Monte Carlo methods are still

slower than approximate schemes, improving their efficiency remains interesting since saved time can then be reinvested in increased convergence or systematic studies.

Acknowledgments

We thank F. Brient for providing us with the FIRE stratocumulus LES field and C. Coustet for useful discussions. We acknowledge support from the Agence Nationale de la Recherche (ANR, grant HIGH-TUNE ANR-16-CE01-0010, <http://www.umr-cnrm.fr/high-tune>), from the french Programme National de Tldtection Spatiale (PNTS-2016-05), from Region Occitanie (Projet CLE-2016 EDStar) and from the French Minister of Higher Education, Research and Innovation for the PhD scholarship of the first author. The data and sources described in this paper are available at <https://www.meso-star.com/projects/high-tune/high-tune.html>.

References

- Alkasem, A., Szczap, F., Cornet, C., Shcherbakov, V., Gour, Y., Jourdan, O., . . . Mioche, G. (2017, 07). Effects of cirrus heterogeneity on lidar caliop/calipso data. *Journal of Quantitative Spectroscopy and Radiative Transfer*, 202. doi: 10.1016/j.jqsrt.2017.07.005
- Appel, A. (1968). Some techniques for shading machine renderings of solids. In *Proceedings of the april 30–may 2, 1968, spring joint computer conference* (pp. 37–45). New York, NY, USA: ACM. doi: 10.1145/1468075.1468082
- Arvo, J., & Kirk, D. (1990, September). Particle transport and image synthesis. *SIGGRAPH Comput. Graph.*, 24(4), 63–66. doi: 10.1145/97880.97886
- Barker, H. W., Cole, J. N. S., Li, J., Yi, B., & Yang, P. (2015, November). Estimation of Errors in Two-Stream Approximations of the Solar Radiative Transfer Equation for Cloudy-Sky Conditions. *Journal of the Atmospheric Sciences*, 72(11), 4053–4074. doi: 10.1175/JAS-D-15-0033.1
- Barker, H. W., Stephens, G. L., Partain, P. T., Bergman, J. W., Bonnel, B., Campana, K., . . . others (2003). Assessing 1d atmospheric solar radiative transfer models: Interpretation and handling of unresolved clouds. *Journal of Climate*, 16(16), 2676–2699.
- Barlakas, V., Macke, A., Wendisch, M., & Ehrlich, A. (2014, 06). Implementation of polarization in a 3d monte carlo radiative transfer model. *Wiss Mitt Inst Meteorol Univ Leipz*, 52, 1-14.
- Benner, T. C., & Evans, K. F. (2001). Three-dimensional solar radiative transfer in small tropical cumulus fields derived from high-resolution imagery. *Journal of geophysical research*, 106, 14.
- Brown, A., Cederwall, R., Chlond, A., Duynkerke, P., Golaz, J.-C., Khairoutdinov, M., . . . Stevens, B. (2002). Large-eddy simulation of the diurnal cycle of shallow cumulus convection over land. *Q. J. R. Meteorol. Soc.*, 128, 1075–1093.
- Buras, R., & Mayer, B. (2011, February). Efficient unbiased variance reduction techniques for Monte Carlo simulations of radiative transfer in cloudy atmospheres: The solution. *Journal of Quantitative Spectroscopy and Radiative Transfer*, 112(3), 434–447. doi: 10.1016/j.jqsrt.2010.10.005
- Cahalan, R. F., Oreopoulos, L., Marshak, A., Evans, K. F., Davis, A. B., Pincus, R., . . . Zhuravleva, T. B. (2005, September). THE I3rc: Bringing Together the Most Advanced Radiative Transfer Tools for Cloudy Atmospheres. *Bulletin of the American Meteorological Society*, 86(9), 1275–1293. doi: 10.1175/BAMS-86-9-1275
- Cess, R., Potter, G., Blanchet, J.-P., J Boer, G., Ghan, S., Kiehl, J., . . . Yagai, I. (1989, 09). Interpretation of cloud-climate feedback as produced by 14 atmospheric general circulation models. , 245, 513-6.
- Cole, J. (2005). *Assessing the importance of unresolved cloud-radiation interactions in atmospheric global climate models using the multiscale modelling framework* (Unpublished doctoral dissertation). Pennsylvania State University.
- Coleman, W. A. (1968). Mathematical verification of a certain monte carlo sampling technique and applications of the technique to radiation transport problems. *Nuclear Science and Engineering*, 32(1), 76-81. doi: 10.13182/NSE68-1
- Collins, D. G., & Wells, M. B. (1965). *Monte carlo codes for study of light transport in the atmosphere. vol i: Description of codes* (Tech. Rep.). U.S. Department of Commerce, Institute for Applied Technology.
- Cook, R. L., Porter, T., & Carpenter, L. (1984, January). Distributed ray tracing. *SIGGRAPH Comput. Graph.*, 18(3), 137–145. doi: 10.1145/964965.808590
- Cornet, C., C-Labonnote, L., Waquet, F., Szczap, F., Deaconu, L., Parol, F., . . . Riédi, J. (2018). Cloud heterogeneity on cloud and aerosol above cloud properties retrieved from simulated total and polarized reflectances. *Atmospheric Measurement Techniques*, 11(6), 3627–3643. doi: 10.5194/amt-11-3627-2018
- Cornet, C., Labonnote, L., & Szczap, F. (2010). Three-dimensional polarized monte carlo atmospheric radiative transfer model (3dmcpol): 3d effects on polarized visible re-

- reflectances of a cirrus cloud. *Journal of Quantitative Spectroscopy and Radiative Transfer*, *111*(1), 174 - 186. doi: <https://doi.org/10.1016/j.jqsrt.2009.06.013>
- Dauchet, J., Bezian, J.-J., Blanco, S., Caliot, C., Charon, J., Coustet, C., ... Weitz, S. (2018). Addressing nonlinearities in Monte Carlo. *Scientific reports*, *8*, 2045-2322. doi: [10.1038/s41598-018-31574-4](https://doi.org/10.1038/s41598-018-31574-4)
- Dauchet, J., Blanco, S., Cornet, J.-F., Hafi, M. E., Eymet, V., & Fournier, R. (2013). The practice of recent radiative transfer monte carlo advances and its contribution to the field of microorganisms cultivation in photobioreactors. *Journal of Quantitative Spectroscopy and Radiative Transfer*, *128*, 52 - 59. (Eurotherm Seminar on Computational Thermal Radiation in Participating Media IV) doi: <https://doi.org/10.1016/j.jqsrt.2012.07.004>
- Davies, R. (1978). The Effect of Finite Geometry on the Three-Dimensional Transfer of Solar Irradiance in Clouds. *Journal Of The Atmospheric Sciences*, *35*(9), 1712-1725.
- Davis, A., Wiscombe, W., Cahalan, R., & Marshak, A. (1994, 04). Multifractal characterizations of nonstationary and intermittency in geophysical fields: Observed, retrieved, or simulated. *Journal of Geophysical Research*, *99*, 8055-8072. doi: [10.1029/94JD00219](https://doi.org/10.1029/94JD00219)
- de Lataillade, A., Blanco, S., Clergent, Y., Dufresne, J., Hafi, M. E., & Fournier, R. (2002). Monte carlo method and sensitivity estimations. *Journal of Quantitative Spectroscopy and Radiative Transfer*, *75*(5), 529 - 538. doi: [https://doi.org/10.1016/S0022-4073\(02\)00027-4](https://doi.org/10.1016/S0022-4073(02)00027-4)
- Delatorre, J., Baud, G., Bzian, J., Blanco, S., Caliot, C., Cornet, J., ... Weitz, S. (2014). Monte carlo advances and concentrated solar applications. *Solar Energy*, *103*, 653 - 681. doi: <https://doi.org/10.1016/j.solener.2013.02.035>
- Deutschmann, T., Beirle, S., Frie, U., Grzegorski, M., Kern, C., Kritten, L., ... Pfeilsticker, K. (2011). The monte carlo atmospheric radiative transfer model mcartim: Introduction and validation of jacobians and 3d features. *Journal of Quantitative Spectroscopy and Radiative Transfer*, *112*(6), 1119 - 1137. doi: <https://doi.org/10.1016/j.jqsrt.2010.12.009>
- Dufresne, J.-L., & Bony, S. (2008). An assessment of the primary sources of spread of global warming estimates from coupled atmosphereocean models. *Journal of Climate*, *21*(19), 5135-5144. doi: [10.1175/2008JCLI2239.1](https://doi.org/10.1175/2008JCLI2239.1)
- Duynkerke, P. G., de Roode, S. R., van Zanten, M. C., Calvo, J., Cuxart, J., Cheinet, S., ... Sednev, I. (2004). Observations and numerical simulations of the diurnal cycle of the eurocs stratocumulus case. *Quarterly Journal of the Royal Meteorological Society*, *130*(604), 3269-3296. doi: [10.1256/qj.03.139](https://doi.org/10.1256/qj.03.139)
- Emde, C., Barlakas, V., Cornet, C., Evans, F., Korkin, S., Ota, Y., ... Wendisch, M. (2015). Iprt polarized radiative transfer model intercomparison project phase a. *Journal of Quantitative Spectroscopy and Radiative Transfer*, *164*, 8 - 36. doi: <https://doi.org/10.1016/j.jqsrt.2015.05.007>
- Emde, C., Barlakas, V., Cornet, C., Evans, F., Wang, Z., Labonotte, L. C., ... Wendisch, M. (2018). Iprt polarized radiative transfer model intercomparison project three-dimensional test cases (phase b). *Journal of Quantitative Spectroscopy and Radiative Transfer*, *209*, 19 - 44. doi: <https://doi.org/10.1016/j.jqsrt.2018.01.024>
- Evans, K. F. (1998, February). The Spherical Harmonics Discrete Ordinate Method for Three-Dimensional Atmospheric Radiative Transfer. *Journal of the Atmospheric Sciences*, *55*(3), 429-446. doi: [10.1175/1520-0469\(1998\)055<0429:TSHDOM>2.0.CO;2](https://doi.org/10.1175/1520-0469(1998)055<0429:TSHDOM>2.0.CO;2)
- Eymet, V., Fournier, R., Blanco, S., & Dufresne, J.-L. (2005, 02). A boundary-based net-exchange monte carlo method for absorbing and scattering thick media. *Journal of Quantitative Spectroscopy and Radiative Transfer*, *91*, 27-46. doi: [10.1016/j.jqsrt.2004.05.049](https://doi.org/10.1016/j.jqsrt.2004.05.049)
- Eymet, V., Poitou, D., Galtier, M., El-Hafi, M., Terree, G., & Fournier, R. (2013, November). Null-collision meshless Monte-Carlo —Application to the validation of fast radiative transfer solvers embedded in combustion simulators. *Journal of Quantitative Spectroscopy and Radiative Transfer*, *129*, 145-157. doi: [10.1016/j.jqsrt.2013.06.004](https://doi.org/10.1016/j.jqsrt.2013.06.004)
- Fauchez, T., Cornet, C., Szczap, F., Dubuisson, P., & Rosambert, T. (2014). Impact of cirrus

- clouds heterogeneities on top-of-atmosphere thermal infrared radiation. *Atmospheric Chemistry and Physics*, *14*(11), 5599–5615. doi: 10.5194/acp-14-5599-2014
- Fournier, R., Blanco, S., Eymet, V., Mouna, E. H., & Spiesser, C. (2016, 02). Radiative, conductive and convective heat-transfers in a single monte carlo algorithm. , *676*, 012007.
- Fu, Q., & Liou, K. N. (1992). On the correlated k-distribution method for Radiative Transfer in nonhomogeneous atmospheres. *Journal of the Atmospheric Sciences*, *49*, 2139–2156.
- Galtier, M., Blanco, S., Caliot, C., Coustet, C., Dauchet, J., El Hafi, M., ... Terre, G. (2013, August). Integral formulation of null-collision Monte Carlo algorithms. *Journal of Quantitative Spectroscopy and Radiative Transfer*, *125*, 57–68. doi: 10.1016/j.jqsrt.2013.04.001
- Galtier, M., Blanco, S., Dauchet, J., Hafi, M. E., Eymet, V., Fournier, R., ... Terre, G. (2016). Radiative transfer and spectroscopic databases: A line-sampling monte carlo approach. *Journal of Quantitative Spectroscopy and Radiative Transfer*, *172*, 83 - 97. (Eurotherm Conference No. 105: Computational Thermal Radiation in Participating Media V) doi: <https://doi.org/10.1016/j.jqsrt.2015.10.016>
- Galtier, M., Roger, M., André, F., & Delmas, A. (2017, July). A symbolic approach for the identification of radiative properties. *Journal of Quantitative Spectroscopy and Radiative Transfer*, *196*, 130-141. doi: 10.1016/j.jqsrt.2017.03.026
- Glouchkov, D., Koshelev, K., & Schulz, A. (2003). Monte carlo simulation of photon transport for optically thick, differentially moving plasmas: Ii. escape factors for differentially moving spheres. *Journal of Quantitative Spectroscopy and Radiative Transfer*, *81*(1), 191 - 197. (Radiative Properties of Hot Dense Matter) doi: [https://doi.org/10.1016/S0022-4073\(03\)00071-2](https://doi.org/10.1016/S0022-4073(03)00071-2)
- Harshvardhan, Weinman, J. A., & Davies, R. (1981, November). Transport of Infrared Radiation in Cuboidal Clouds. *Journal of the Atmospheric Sciences*, *38*(11), 2500–2513. doi: 10.1175/1520-0469(1981)038<2500:TOIRIC>2.0.CO;2
- Hinkelman, L. M., Evans, K. F., Clothiaux, E. E., Ackerman, T. P., & Stackhouse, P. W. (2007). The effect of cumulus cloud field anisotropy on domain-averaged solar fluxes and atmospheric heating rates. *Journal of the Atmospheric Sciences*, *64*(10), 3499-3520. doi: 10.1175/JAS4032.1
- Hogan, R. J., Ahlgrimm, M., Balsamo, G., Beljaars, A., Berrisford, P., Bozzo, A., ... Wedi, N. (2017, 2017). Radiation in numerical weather prediction. *ECMWF Technical Memorandum*(816).
- Hogan, R. J., & Bozzo, A. (2018). A flexible and efficient radiation scheme for the ECMWF model. *Journal of Advances in Modeling Earth Systems*. doi: 10.1029/2018MS001364
- Hogan, R. J., Schäfer, S. A. K., Klinger, C., Chiu, J. C., & Mayer, B. (2016, July). Representing 3-D cloud radiation effects in two-stream schemes: 2. Matrix formulation and broadband evaluation. *Journal of Geophysical Research: Atmospheres*, *121*(14), 2016JD024875. doi: 10.1002/2016JD024875
- Iacono, M. J., Delamere, J. S., Mlawer, E. J., Shephard, M. W., Clough, S. A., & Collins, W. D. (2008). Radiative forcing by long-lived greenhouse gases: Calculations with the aer radiative transfer models. *Journal of Geophysical Research: Atmospheres*, *113*(D13). doi: 10.1029/2008JD009944
- Iwabuchi, H. (2006). Efficient Monte Carlo methods for radiative transfer modeling. *Journal of the atmospheric sciences*, *63*(9), 2324–2339.
- Iwabuchi, H., & Kobayashi, H. (2006). *Modeling of radiative transfer in cloudy atmospheres and plant canopies using monte carlo methods* (Vol. 7; Tech. Rep.). Japan Agency for Marine-Earth Science and Technology (JAMSTEC).
- Jones, A. L., & Di Girolamo, L. (2018). Design and verification of a new monochromatic thermal emission component for the i3rc community monte carlo model. *Journal of the Atmospheric Sciences*, *75*(3), 885-906. doi: 10.1175/JAS-D-17-0251.1
- Joseph, J. H., Wiscombe, W. J., & Weinman, J. A. (1976, December). The Delta-Eddington Approximation for Radiative Flux Transfer. *Journal of the Atmospheric Sciences*,

- 33(12), 2452–2459. doi: 10.1175/1520-0469(1976)033<2452:TDEAFR>2.0.CO;2
- Kajiya, J. T. (1986, August). The rendering equation. *SIGGRAPH Comput. Graph.*, 20(4), 143–150. doi: 10.1145/15886.15902
- Kassianov, E. I., & Kogan, Y. L. (2002). Spectral dependence of radiative horizontal transport in stratocumulus clouds and its effect on near-ir absorption. *Journal of Geophysical Research: Atmospheres*, 107(D23), AAC 15-1-AAC 15-13. doi: 10.1029/2002JD002103
- Kato, S., & Marshak, A. (2009). Solar zenith and viewing geometry-dependent errors in satellite retrieved cloud optical thickness: Marine stratocumulus case. *Journal of Geophysical Research: Atmospheres*, 114(D1). doi: 10.1029/2008JD010579
- Klinger, C., Feingold, G., & Yamaguchi, T. (2018). Cloud droplet growth in shallow cumulus clouds considering 1d and 3d thermal radiative effects. *Atmospheric Chemistry and Physics Discussions*, 2018, 1–29. doi: 10.5194/acp-2018-1204
- Klinger, C., Mayer, B., Jakub, F., Zinner, T., Park, S.-B., & Gentine, P. (2017). Effects of 3-d thermal radiation on the development of a shallow cumulus cloud field. *Atmospheric Chemistry and Physics*, 17(8), 5477–5500. doi: 10.5194/acp-17-5477-2017
- Knuth, D. E. (1984). Literate programming. *The Computer Journal*, 27(2), 97–111. doi: 10.1093/comjnl/27.2.97
- Kobayashi, H., & Iwabuchi, H. (2008, 01). A coupled 1-d atmosphere and 3-d canopy radiative transfer model for canopy reflectance, light environment, and photosynthesis simulation in a heterogeneous landscape. *Remote Sensing of Environment*, 112, 173–185. doi: 10.1016/j.rse.2007.04.010
- Koura, K. (1986). Nullcollision technique in the directsimulation monte carlo method. *The Physics of Fluids*, 29(11), 3509–3511. doi: 10.1063/1.865826
- Kutz, P., Habel, R., Li, Y. K., & Novák, J. (2017, July). Spectral and decomposition tracking for rendering heterogeneous volumes. *ACM Trans. Graph.*, 36(4), 111:1–111:16. doi: 10.1145/3072959.3073665
- Lac, C., Chaboureaud, J.-P., Masson, V., Pinty, J.-P., Tulet, P., Escobar, J., ... Wautelet, P. (2018). Overview of the meso-nh model version 5.4 and its applications. *Geoscientific Model Development*, 11(5), 1929–1969. doi: 10.5194/gmd-11-1929-2018
- Macke, A., Mitchell, D., & Bremen, L. (1999). Monte Carlo radiative transfer calculations for inhomogeneous mixed phase clouds. *Physics and Chemistry of the Earth B*, 24, 237–241. doi: 10.1016/S1464-1909(98)00044-6
- Marchuk, G. I., Mikhailov, G. A., Nazaraliev, M. A., Darbinjan, R. A., Kargin, B. A., & Elepov, B. S. (1980). Elements of Radiative-Transfer Theory Used in the Monte Carlo Methods. In *The Monte Carlo Methods in Atmospheric Optics* (pp. 5–17). Springer, Berlin, Heidelberg. (DOI: 10.1007/978-3-540-35237-2.2)
- Marchuk, G. I., Mikhailov, G. A., Nazareliev, M. A., Darbinjan, R. A., Kargin, B. A., & Elepov, B. S. (1980). *The Monte Carlo Methods in Atmospheric Optics*. Berlin Heidelberg: Springer-Verlag.
- Marshak, A., & Davis, A. (Eds.). (2005). *3d Radiative Transfer in Cloudy Atmospheres*. Berlin Heidelberg: Springer-Verlag. (DOI: 10.1007/3-540-28519-9)
- Marshak, A., Davis, A., Wiscombe, W., & Cahalan, R. (1995). Radiative smoothing in fractal clouds. *Journal of Geophysical Research: Atmospheres*, 100(D12), 26247–26261. doi: 10.1029/95JD02895
- Mayer, B., & Kylling, A. (2005). Technical note: The libradtran software package for radiative transfer calculations - description and examples of use. *Atmospheric Chemistry and Physics*, 5(7), 1855–1877. doi: 10.5194/acp-5-1855-2005
- McKee, T. B., & Klehr, J. T. (1978). Effects of Cloud Shape on Scattered Solar Radiation. *Monthly Weather Review*, 106(3), 399–404. doi: 10.1175/1520-0493(1978)106<0399:EOCSOS>2.0.CO;2
- Mikhailov, G., & Sabelfeld, K. (1995). *Optimization of weighted monte carlo methods*. Springer Berlin Heidelberg.
- Mishchenko, M., D. Travis, L., & Lacis, A. (2002). *Scattering, absorption, and emission of light by small particles* (Vol. 4).

- Mlawer, E. J., Taubman, S. J., Brown, P. D., Iacono, M. J., & Clough, S. A. (1997, July). Radiative transfer for inhomogeneous atmospheres: RRTM, a validated correlated-k model for the longwave. *Journal of Geophysical Research: Atmospheres*, *102*(D14), 16663–16682. doi: 10.1029/97JD00237
- Novák, J., Georgiev, I., Hanika, J., & Jarosz, W. (2018, May). Monte Carlo Methods for Volumetric Light Transport Simulation. *Computer Graphics Forum*, *37*(2), 551–576. doi: 10.1111/cgf.13383
- Novák, J., Selle, A., & Jarosz, W. (2014, November). Residual ratio tracking for estimating attenuation in participating media. *ACM Transactions on Graphics (Proceedings of ACM SIGGRAPH Asia 2014)*, *33*(6), 179:1–179:11.
- OHirok, W., & Gautier, C. (1998). A three-dimensional radiative transfer model to investigate the solar radiation within a cloudy atmosphere. part i: Spatial effects. *Journal of the Atmospheric Sciences*, *55*(12), 2162–2179. doi: 10.1175/1520-0469(1998)055<2162:ATDRTM>2.0.CO;2
- Pharr, M., & Humphreys, G. (2018). *Physically based rendering, third edition: From theory to implementation* (3rd ed.). Retrieved from <http://www.pbr-book.org/>
- Pincus, R., & Evans, K. F. (2009, October). Computational Cost and Accuracy in Calculating Three-Dimensional Radiative Transfer: Results for New Implementations of Monte Carlo and SHDOM. *Journal of the Atmospheric Sciences*, *66*(10), 3131–3146. doi: 10.1175/2009JAS3137.1
- Pincus, R., Hannay, C., & Evans, K. F. (2005). The accuracy of determining three-dimensional radiative transfer effects in cumulus clouds using ground-based profiling instruments. *Journal of the atmospheric sciences*, *62*(7), 2284–2293.
- Raab, M., Seibert, D., & Keller, A. (2006). Unbiased global illumination with participating media. In A. Keller, S. Heinrich, & H. Niederreiter (Eds.), *Monte carlo and quasi-monte carlo methods 2006* (pp. 591–605). Berlin, Heidelberg: Springer Berlin Heidelberg.
- Ramanathan, V., Cess, R. D., Harrison, E. F., Minnis, P., Barkstrom, B. R., Ahmad, E., & Hartmann, D. (1989). Cloud-radiative forcing and climate: Results from the earth radiation budget experiment. *Science*, *243*(4887), 57–63. doi: 10.1126/science.243.4887.57
- Roger, M., Blanco, S., Mouna, E. H., & Fournier, R. (2005, 11). Monte carlo estimates of domain-deformation sensitivities. , *95*, 180601.
- Rossow, W. B., & Dugas, E. N. (2004). The international satellite cloud climatology project (isccp) web site: An online resource for research. *Bulletin of the American Meteorological Society*, *85*(2), 167–172.
- Schäfer, S. (2016). *What is the global impact of 3d cloud-radiation interactions ?* (Unpublished doctoral dissertation). University of Reading, Reading, England.
- Schäfer, S. A. K., Hogan, R. J., Klinger, C., Chiu, J. C., & Mayer, B. (2016, July). Representing 3-D cloud radiation effects in two-stream schemes: 1. Longwave considerations and effective cloud edge length. *Journal of Geophysical Research: Atmospheres*, *121*(14), 2016JD024876. doi: 10.1002/2016JD024876
- Shonk, J. K. P., & Hogan, R. J. (2008, june). Tripleclouds: An Efficient Method for Representing Horizontal Cloud Inhomogeneity in 1d Radiation Schemes by Using Three Regions at Each Height. *Journal of Climate*, *21*(11), 2352–2370. doi: 10.1175/2007JCLI1940.1
- Siebesma, A. P., Bretherton, C. S., Brown, A., Chlond, A., Cuxart, J., Duynkerke, P. G., ... Stevens, D. E. (2003). A large eddy simulation intercomparison study of shallow cumulus convection. *Journal of the Atmospheric Sciences*, *60*(10), 1201–1219.
- Skullerud, H. R. (1968, November). The stochastic computer simulation of ion motion in a gas subjected to a constant electric field. *Journal of Physics D Applied Physics*, *1*, 1567–1568. doi: 10.1088/0022-3727/1/11/423
- Spanier, J., & Gelbard, E. M. (2008). *Monte carlo principles and neutron transport problems*. Courier Corporation.
- Szczap, F., Cornet, C., Alqassem, A., Gour, Y., C-Labonnote, L., & Jourdan, O. (2013).

- A 3D polarized Monte Carlo LIDAR system simulator for studying effects of cirrus inhomogeneities on CALIOP/CALIPSO measurements. *AIP Conference Proceedings*, 1531(1), 139-142. doi: 10.1063/1.4804727
- Takara, E. E., & Ellingson, R. G. (1996, May). Scattering Effects on Longwave Fluxes in Broken Cloud Fields. *Journal of the Atmospheric Sciences*, 53(10), 1464-1476. doi: 10.1175/1520-0469(1996)053<1464:SEOLFI>2.0.CO;2
- Várnai, T., & Marshak, A. (2003). A method for analyzing how various parts of clouds influence each other's brightness. *Journal of Geophysical Research: Atmospheres*, 108(D22). doi: 10.1029/2003JD003561
- Veach, E. (1998). *Robust monte carlo methods for light transport simulation* (Unpublished doctoral dissertation). Stanford, CA, USA. (AAI9837162)
- Veach, E., & Guibas, L. (1995, 01). Bidirectional estimators for light transport. *Proceedings of Eurographics Workshop on Rendering*. doi: 10.1007/978-3-642-87825-1_11
- Veach, E., & Guibas, L. J. (1997). Metropolis light transport. , 65-76. doi: 10.1145/258734.258775
- Wald, I. (2004). *Realtime ray tracing and its use for interactive global illumination* (Unpublished doctoral dissertation).
- Wald, I., Slusallek, P., Benthin, C., & Wagner, M. (2001). Interactive rendering with coherent ray tracing. In *Computer graphics forum* (pp. 153-164).
- Wald, I., Woop, S., Benthin, C., Johnson, G. S., & Ernst, M. (2014, July). Embree: A kernel framework for efficient cpu ray tracing. *ACM Trans. Graph.*, 33(4), 143:1-143:8. doi: 10.1145/2601097.2601199
- Weise, K., & Zhang, H. (1997). Uncertainty treatment in monte carlo simulation. *Journal of Physics A: Mathematical and General*, 30(17), 5971.
- Whitted, T. (1980, June). An improved illumination model for shaded display. *Commun. ACM*, 23(6), 343-349. doi: 10.1145/358876.358882
- Woodcock, E., Murphy, T., Hemmings, P., & Longworth, S. (1965). Techniques used in the gem code for monte carlo neutronics calculations in reactors and other systems of complex geometry. , 557.
- Yue, Y., Iwasaki, K., Chen, B.-Y., Dobashi, Y., & Nishita, T. (2011). Toward optimal space partitioning for unbiased, adaptive free path sampling of inhomogeneous participating media. *Computer Graphics Forum*, 30(7), 1911-1919. doi: 10.1111/j.1467-8659.2011.02049.x